

**Singlet model interference effects with high scale UV physics**S. Dawson<sup>1</sup> and I. M. Lewis<sup>2</sup><sup>1</sup>*Department of Physics, Brookhaven National Laboratory, Upton, New York 11973, USA*<sup>2</sup>*Department of Physics and Astronomy, University of Kansas, Lawrence, Kansas 66045, USA*

(Received 23 May 2016; published 6 January 2017)

One of the simplest extensions of the Standard Model (SM) is the addition of a scalar gauge singlet,  $S$ . If  $S$  is not forbidden by a symmetry from mixing with the Standard Model Higgs boson, the mixing will generate non-SM rates for Higgs production and decays. In general, there could also be unknown high energy physics that generates additional effective low energy interactions. We show that interference effects between the scalar resonance of the singlet model and the effective field theory (EFT) operators can have significant effects in the Higgs sector. We examine a non- $Z_2$  symmetric scalar singlet model and demonstrate that a fit to the 125 GeV Higgs boson couplings and to limits on high mass resonances,  $S$ , exhibit an interesting structure and possible large cancellations of effects between the resonance contribution and the new EFT interactions, that invalidate conclusions based on the renormalizable singlet model alone.

DOI: 10.1103/PhysRevD.95.015004

**I. INTRODUCTION**

Among the simplest extensions of the Standard Model (SM) is the addition of a gauge singlet scalar particle,  $S$ . The singlet particle couples to SM particles through its mixing with the SM-like 125 GeV Higgs boson. In general, there can be additional interactions between the  $S$  and the gauge bosons, which can be parametrized as effective field theory (EFT) dimension-5 couplings. The source of these effective interactions is not relevant for our discussion, and our focus is on the consequences of the interference effects between the heavy scalar resonance and the EFT operators. Since there are a relatively few number of EFT operators coupling the singlet to the  $SU(3) \times SU(2) \times U(1)$  gauge bosons, it is possible to obtain interesting limits on the theory, despite the addition of new parameters.

In the absence of a  $Z_2$  symmetry, the singlet model allows cubic and linear self-coupling terms in the scalar potential and a strong first order electroweak phase transition is possible for certain values of the parameter space [1–5], making this theory highly motivated phenomenologically. We begin by examining restrictions on the parameters of the non- $Z_2$  symmetric model from the measured 125 GeV Higgs couplings and from the requirement that the electroweak minimum be the absolute minima of the potential. We then include LHC limits on heavy resonances that decay into SM particles (assuming that there are no additional light particles). Novel features of our analysis are the insistence that the parameters satisfy the minimization condition of the potential and our inclusion of interference effects between the SM contributions to the Higgs widths and the contributions from the EFT interactions.

These interference effects can be large and significantly change the allowed regions of parameter space.

In Sec. II, we review the singlet model and the EFT interactions, along with compact expressions for the decay widths. Section III discusses constraints from the 125 GeV Higgs, and Sec. IV contains our limits on the properties of both the 125 scalar and EFT coefficients, and a discussion of the size of the allowed mixing between the SM-like and heavy scalars in the presence of EFT coefficients. Section V contains some conclusions.

**II. MODEL CONSIDERATIONS****A. Singlet plus EFT Model**

We consider a model containing the SM Higgs doublet,  $H$ , and an additional scalar singlet,  $S$ . The most general renormalizable scalar potential is

$$V(H, S) = -\mu^2 H^\dagger H + \lambda (H^\dagger H)^2 + \frac{a_1}{2} H^\dagger H S + \frac{a_2}{2} H^\dagger H S^2 + b_1 S + \frac{b_2}{2} S^2 + \frac{b_3}{3} S^3 + \frac{b_4}{4} S^4. \quad (1)$$

The singlet model has been examined in some detail in the literature [1,2,6–12] and so our discussion is appropriately brief. If there is a  $Z_2$  symmetry  $S \rightarrow -S$ , then  $a_1 = b_1 = b_3 = 0$ . The  $Z_2$  nonsymmetric model is, however, particularly interesting since it is possible to arrange the parameters in such a way as to obtain a strong first order phase transition [1–5,13].

The neutral scalar components of the doublet  $H$  and singlet  $S$  are denoted by  $\phi_0 = (h + v)/\sqrt{2}$  and  $S = s + x$ , where the vacuum expectation values are  $\langle \phi_0 \rangle = \frac{v}{\sqrt{2}}$  and  $\langle S \rangle = x$ . We require that the global minimum of the

potential correspond to the electroweak symmetry breaking (EWSB) minimum,  $v = v_{\text{EW}} = 246$  GeV [1,9], which places significant constraints on the allowed parameters. Note that a shift of the singlet field by  $S \rightarrow S + \Delta_S$  is just a redefinition of the parameters of Eq. (1), and we are free to choose our electroweak symmetry breaking minimum as  $(v, x) \equiv (v_{\text{EW}}, 0)$ .<sup>1</sup>

The physical scalars are mixtures of  $h$  and  $s$ , and the scalar mixing is parametrized as

$$\begin{pmatrix} h_1 \\ h_2 \end{pmatrix} = \begin{pmatrix} \cos \theta & \sin \theta \\ -\sin \theta & \cos \theta \end{pmatrix} \begin{pmatrix} h \\ s \end{pmatrix}, \quad (2)$$

where  $h_{1,2}$  are the mass eigenstates with masses  $m_1, m_2$ . The parameters of the scalar potential can be solved for in terms of the physical masses and mixing,

$$\begin{aligned} a_1 &= \frac{m_1^2 - m_2^2}{v} \sin 2\theta, \\ b_2 + \frac{a_2}{2} v^2 &= m_1^2 \sin^2 \theta + m_2^2 \cos^2 \theta, \\ \lambda &= \frac{m_1^2 \cos^2 \theta + m_2^2 \sin^2 \theta}{2v^2} \\ \mu^2 &= \lambda v^2 \\ b_1 &= -\frac{v^2}{4} a_1. \end{aligned} \quad (3)$$

Our free parameters are then

$$\begin{aligned} m_1 &= 125 \text{ GeV}, \quad m_2, \theta, v_{\text{EW}} = 246 \text{ GeV}, \\ x &= 0, a_2, b_3, b_4. \end{aligned} \quad (4)$$

The couplings of the  $h_1$  to SM particles are suppressed by  $\cos \theta$  and both ATLAS and CMS have obtained limits from the measured couplings. ATLAS finds at 95% confidence level,  $\sin \theta \leq .35$ , assuming no branching ratio to invisible particles [14]. Using the fitted global signal strength for the SM Higgs boson,  $\mu = 1.03^{+0.17}_{-0.15}$  [15], a 95% confidence level limit can be extracted,  $\sin \theta \leq .51$ . In the absence of the EFT coefficients, a fit to the oblique parameters also restricts  $\sin \theta$  [2,8,9,16], but the limit from Higgs coupling measurements is stronger.

The limits on  $\sin \theta$  can be significantly altered, however, when the EFT operators are included. We postulate the  $SU(3) \times SU(2) \times U(1)$  gauge invariant effective interactions,

$$L = g_s^2 \frac{c_{gg}}{\Lambda} S G^{\mu\nu, A} G_{\mu\nu}^A + \frac{c_{WW}}{\Lambda} g^2 S W^{\mu\nu, a} W_{\mu\nu}^a + \frac{c_{BB}}{\Lambda} g'^2 S B^{\mu\nu} B_{\mu\nu}, \quad (5)$$

<sup>1</sup>This freedom to set  $x = 0$  does not occur in the  $Z_2$  symmetric case.

that are assumed to arise from unknown UV physics at a scale  $\Lambda$ . The scalar couplings to gauge bosons are suppressed by the appropriate factor of  $\cos \theta$  or  $\sin \theta$  and receive additional contributions from the interactions of Eq. (5). There is an interplay of effects between the singlet-SM mixing of Eq. (2) and the EFT contributions from Eq. (5), which requires that we fit the data to the complete model [17,18].

Finally, we need the self-interactions of the Higgs bosons in the basis of the mass eigenstates  $h_1$  and  $h_2$ ,

$$V_{\text{self}} \supset \frac{\lambda_{111}}{3!} h_1^3 + \frac{\lambda_{211}}{2!} h_2 h_1^2 + \dots \quad (6)$$

where [8,9]

$$\begin{aligned} \lambda_{111} &= 2s_\theta^3 b_3 + \frac{3a_1}{2} s_\theta c_\theta^2 + 3a_2 s_\theta^2 c_\theta v + 6c_\theta^3 \lambda v, \\ \lambda_{211} &= 2s_\theta^2 c_\theta b_3 + \frac{a_1}{2} c_\theta (c_\theta^2 - 2s_\theta^2) \\ &\quad + (2c_\theta^2 - s_\theta^2) s_\theta v a_2 - 6\lambda s_\theta c_\theta^2 v. \end{aligned} \quad (7)$$

and we abbreviate  $s_\theta = \sin \theta$ ,  $c_\theta = \cos \theta$  and assume  $\sin \theta > 0$ . In the small angle limit, to  $\mathcal{O}(s_\theta^2)$ ,

$$\begin{aligned} \lambda_{111} &\rightarrow 6\lambda v + \frac{3}{2} a_1 s_\theta + 3v s_\theta^2 (a_2 - 3\lambda) \\ &\sim \frac{3m_1^2}{v} + s_\theta^2 \frac{3}{2v} (m_2^2 - 4m_1^2 + 2a_2 v^2) \end{aligned} \quad (8)$$

$$\begin{aligned} \lambda_{211} &\rightarrow \frac{a_1}{2} + s_\theta v (-6\lambda + 2a_2) + \frac{s_\theta^2}{4} (8b_3 - 7a_1) \\ &\sim s_\theta \left( -\frac{3m_1^2}{v} + 2v a_2 \right) + \frac{s_\theta c_\theta}{2v} (m_1^2 - m_2^2) + 2b_3 s_\theta^2. \end{aligned} \quad (9)$$

The restrictions on the parameters of the potential due to the requirement that the electroweak minimum be a global minimum were examined in Ref. [1,9]. In Fig. 1, we fix  $b_4 = 1$ ,  $\cos \theta = .94$  and show the allowed regions for  $a_2$  and  $b_3$  for different values of the heavy scalar mass,  $m_2$ . The areas of these regions increase with  $b_4$ , and the edges of the contours are completely fixed by the global minimum requirement as described in Ref. [9].<sup>2</sup> The regions become somewhat larger as  $m_2$  increases for fixed  $b_4$ . In the softly broken  $Z_2$  scenario of Ref. [5], a first order electroweak phase transition requires  $a_2 > \sim 9$ . In the model without a  $Z_2$  symmetry, a strong first order electroweak phase transition appears to be possible for  $a_2 \sim 1$ –2, and negative  $b_3$  [3],

<sup>2</sup>For example, all points within the shaded regions are allowed by the minimization of the potential.

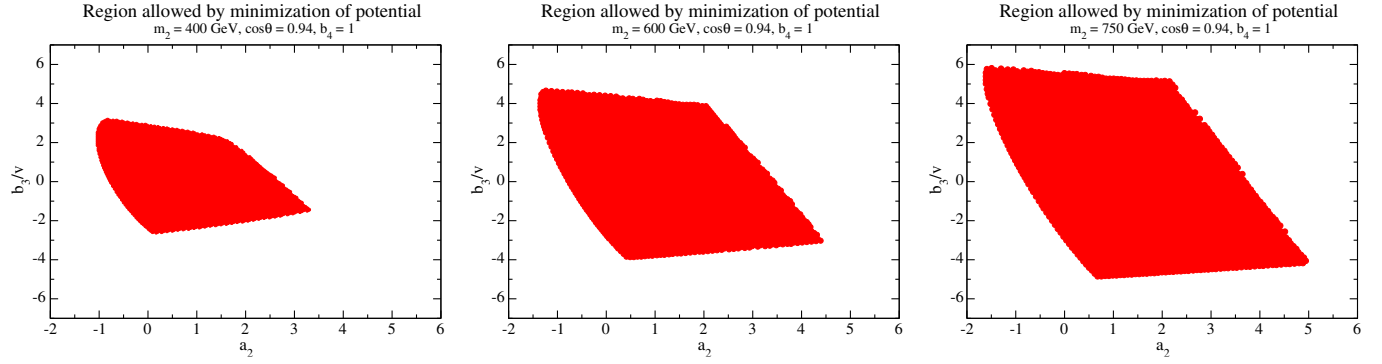


FIG. 1. Regions allowed by the requirement that the electroweak minimum be a global minimum for  $\cos\theta = 0.94$ ,  $b_4 = 1$  and  $m_2 = 400, 600$ , and  $750$  GeV [9].

although the maximum  $m_2$  studied in this reference is  $250$  GeV.

The partial width of  $h_2 \rightarrow h_1 h_1$  is

$$\Gamma(h_2 \rightarrow h_1 h_1) = \frac{\lambda_{211}^2}{32\pi m_2} \sqrt{1 - \frac{4m_1^2}{m_2^2}}. \quad (10)$$

In Fig. 2 we show the partial widths for  $h_2 \rightarrow h_1 h_1$  using the allowed values of  $b_3$  from Fig. 1 for each parameter point for representative values of the parameters. The width can potentially increase significantly as

the resonance mass increases. A measurement of the coupling  $\lambda_{211}$  to sufficient precision could shed light on the values of  $a_2$  and  $b_3$ . We note that in all cases,  $\Gamma(h_2 \rightarrow h_1 h_1)_{\text{max}}/m_2 \sim 1\%$ , and so we are in a narrow width scenario.

## B. Results for decay widths

The decays of  $h_1$  and  $h_2$  are affected by the SM doublet-singlet mixing and by the EFT operators. Retaining the interference with the SM contributions, we find for the heavier state the following:

$$\begin{aligned} \Gamma(h_2 \rightarrow \gamma\gamma) &= \frac{e^4 m_2^3}{4\pi} \left| \sin\theta \left( \frac{\sum_i N_{ci} e_i^2 F_i(\tau_{2i})}{32\pi^2 v} \right) + \cos\theta \frac{c_{\gamma\gamma}}{\Lambda} \right|^2 \\ \Gamma(h_2 \rightarrow gg) &= \frac{2g_s^4 m_2^3}{\pi} \left| \sin\theta \frac{\sum_i F_i(\tau_{2i})}{64\pi^2 v} + \cos\theta \frac{c_{gg}}{\Lambda} \right|^2 \\ \Gamma(h_2 \rightarrow ZZ) &= \frac{1}{32\pi} \frac{m_2^3}{v^2} \sqrt{1 - 4x_{2Z}} \left\{ 2^7 \cos^2\theta \frac{c_{ZZ}^2 M_Z^4}{\Lambda^2 v^2} (1 - 4x_{2Z} + 6x_{2Z}^2) \right. \\ &\quad \left. + 3 \cdot 2^5 \cos\theta \sin\theta \frac{c_{ZZ} M_Z^2}{v\Lambda} x_{2Z} (1 - 2x_{2Z}) + \sin^2\theta (1 - 4x_{2Z} + 12x_{2Z}^2) \right\} \\ \Gamma(h_2 \rightarrow Z\gamma) &= \frac{e^4 m_2^3}{2\pi s_W^2 c_W^2} (1 - x_{2Z})^3 \left| \sin\theta \frac{c_W s_W}{32\pi^2 v} (A_F + A_W) - \cos\theta \frac{c_{Z\gamma}}{\Lambda} \right|^2 \\ \Gamma(h_2 \rightarrow W^+ W^-) &= \frac{1}{16\pi} \frac{m_2^3}{v^2} \sqrt{1 - 4x_{2W}} \left\{ 2^7 \cos^2\theta \frac{c_{WW}^2 M_W^4}{\Lambda^2 v^2} (1 - 4x_{2W} + 6x_{2W}^2) \right. \\ &\quad \left. + 3 \cdot 2^5 \cos\theta \sin\theta \frac{c_{WW} M_W^2}{v\Lambda} x_{2W} (1 - 2x_{2W}) + \sin^2\theta (1 - 4x_{2W} + 12x_{2W}^2) \right\} \\ \Gamma(h_2 \rightarrow f\bar{f}) &= \sin^2\theta \Gamma(h \rightarrow f\bar{f})_{\text{SM}}, \end{aligned} \quad (11)$$

where [19–21],

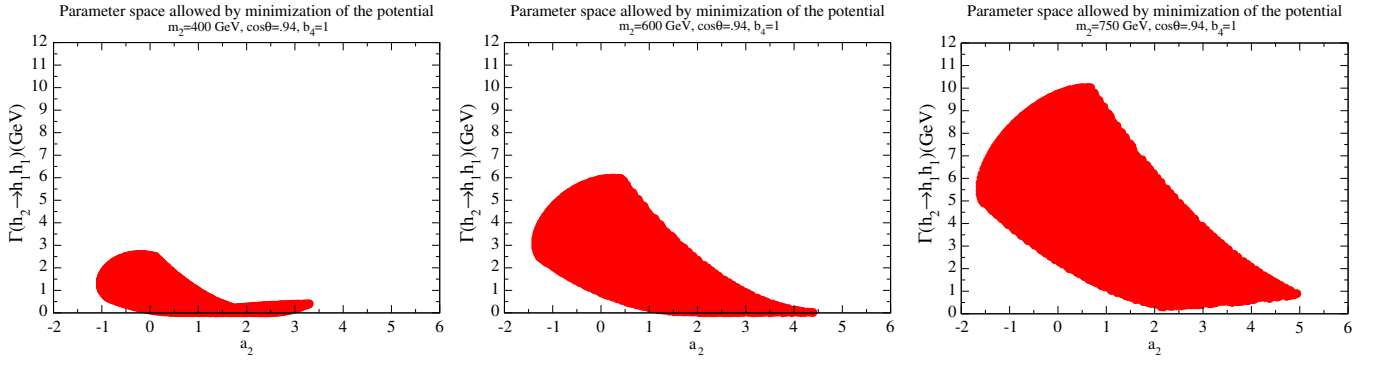


FIG. 2. Allowed decay widths for  $h_2 \rightarrow h_1 h_1$  assuming the parameters correspond to a global minimum of the potential for  $b_4 = 1$ ,  $\cos \theta = 0.94$ , and  $m_2 = 400, 600$  and  $750$  GeV.

$$F_i(\tau_{2i}) = -2\tau_{2i}(1 + (1 - \tau_{2i})f(\tau_{2i})) \text{ for fermions}$$

$$F_W(\tau_{2W}) = 2 + 3\tau_{2W} + 3\tau_{2W}(2 - \tau_{2W})f(\tau_{2W})$$

for gauge bosons

$$x_{iV} = \frac{M_V^2}{m_i^2}$$

$$c_{\gamma\gamma} = c_{WW} + c_{BB}$$

$$c_{ZZ} = c_W^4 c_{WW} + s_W^4 c_{BB}$$

$$c_{Z\gamma} = c_{BB} s_W^2 - c_{WW} c_W^2, \quad (12)$$

and  $e_i$  is the electric charge of particle  $i$ ,  $c_W = M_W/M_Z$ ,  $N_{ci} = 3(1)$  for quarks (leptons),  $\tau_{2i} = \frac{4M_i^2}{m_2^2}$ ,  $M_i$  is the mass of the appropriate fermion or the  $W$  boson,  $A_F$  and  $A_W$  are given in Ref. [19], and

$$f(\tau) = \begin{cases} \left[ \sin^{-1}\left(\frac{1}{\sqrt{\tau}}\right) \right]^2, & \text{if } \tau \geq 1 \\ -\frac{1}{4} \left[ \ln\left(\frac{1 + \sqrt{1 - \tau}}{1 - \sqrt{1 - \tau}}\right) - i\pi \right]^2 & \text{if } \tau < 1. \end{cases} \quad (13)$$

If we consider a model with no mixing with the SM Higgs,  $\sin \theta = 0$ , we have approximately

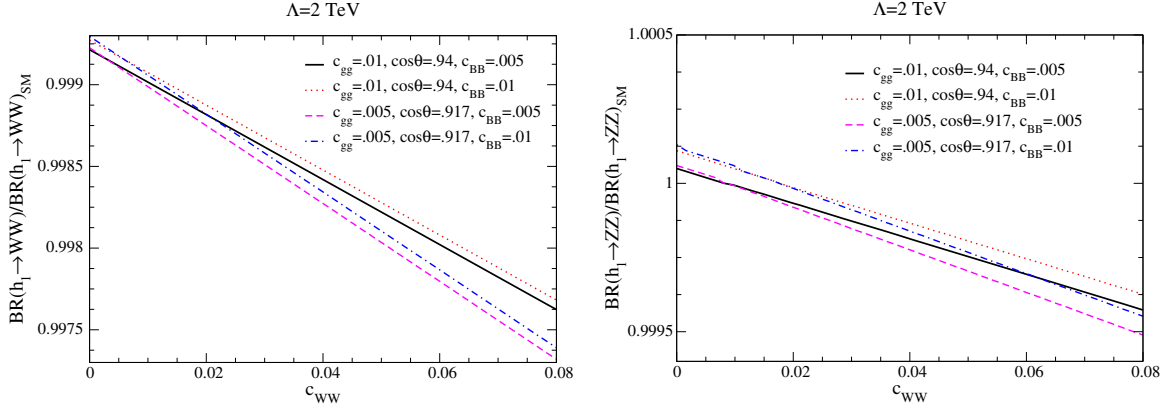
$$\begin{aligned} \Gamma(h_2 \rightarrow \gamma\gamma) &= .04 c_{\gamma\gamma}^2 \left( \frac{m_2}{600 \text{ GeV}} \right)^3 \left( \frac{2 \text{ TeV}}{\Lambda(\text{TeV})} \right)^2 \text{ GeV} \\ \Gamma(h_2 \rightarrow W^+ W^-) &= 0.15 c_{WW}^2 \left( \frac{m_2}{600 \text{ GeV}} \right)^3 \\ &\quad \times \left( \frac{2 \text{ TeV}}{\Lambda(\text{TeV})} \right)^2 \text{ GeV} \\ \Gamma(h_2 \rightarrow ZZ) &= 1.2 c_{ZZ}^2 \left( \frac{m_2}{600 \text{ GeV}} \right)^3 \left( \frac{2 \text{ TeV}}{\Lambda(\text{TeV})} \right)^2 \text{ GeV} \\ \Gamma(h_2 \rightarrow Z\gamma) &= 0.43 c_{Z\gamma}^2 \left( \frac{m_2}{600 \text{ GeV}} \right)^3 \\ &\quad \times \left( \frac{2 \text{ TeV}}{\Lambda(\text{TeV})} \right)^2 \text{ GeV}. \end{aligned} \quad (14)$$

Note that Eq. (14) is an overconstrained result due to the relations of Eq. (12).

The lighter Higgs boson ( $m_1 = 125$  GeV) decay widths are

$$\begin{aligned} \Gamma(h_1 \rightarrow gg) &= \frac{2g_s^4 m_1^3}{\pi} \left| -\cos \theta \frac{\sum_i F_i(\tau_{1i})}{64\pi^2 v} + \sin \theta \frac{c_{gg}}{\Lambda} \right|^2 \\ \Gamma(h_1 \rightarrow \gamma\gamma) &= \frac{e^4 m_1^3}{4\pi} \left| -\cos \theta \left( \frac{\sum_i N_{ci} e_i^2 F_i(\tau_{1i})}{32\pi^2 v} \right) + \sin \theta \frac{c_{\gamma\gamma}}{\Lambda} \right|^2 \\ \Gamma(h_1 \rightarrow WW^*) &= \frac{18g^2 M_W^4}{\pi^3 v^2 m_1} \left\{ \sin^2 \theta \frac{c_{WW}^2}{v^2 \Lambda^2} m_1^4 I_3(M_W) - \cos \theta \sin \theta \frac{c_{WW}}{4v\Lambda} m_1^2 I_2(M_W) + \frac{1}{64} \cos^2 \theta I_1(M_W) \right\} \\ \Gamma(h_1 \rightarrow ZZ^*) &= \kappa \frac{2g^2 M_Z^4}{c_W^2 \pi^3 v^2 m_1} \left\{ \sin^2 \theta \frac{c_{ZZ}^2}{v^2 \Lambda^2} m_1^4 I_3(M_Z) - \cos \theta \sin \theta \frac{c_{ZZ}}{4v\Lambda} m_1^2 I_2(M_Z) + \frac{1}{64} \cos^2 \theta I_1(M_Z) \right\} \\ \Gamma(h_1 \rightarrow Z\gamma) &= \frac{e^4 m_1^3}{2\pi s_W^2 c_W^2} (1 - x_{1Z})^3 \left| \cos \theta \frac{c_W s_W}{32\pi^2 v} (A_F + A_W) + \sin \theta \frac{c_{Z\gamma}}{\Lambda} \right|^2 \\ \Gamma(h_1 \rightarrow f\bar{f}) &= \cos^2 \theta \Gamma(h \rightarrow f\bar{f})_{\text{SM}} \end{aligned} \quad (15)$$

where,

FIG. 3. Branching ratio for (left-hand side)  $h_1 \rightarrow WW$ , and (right-hand side)  $h_1 \rightarrow ZZ$  for representative values of the parameters.

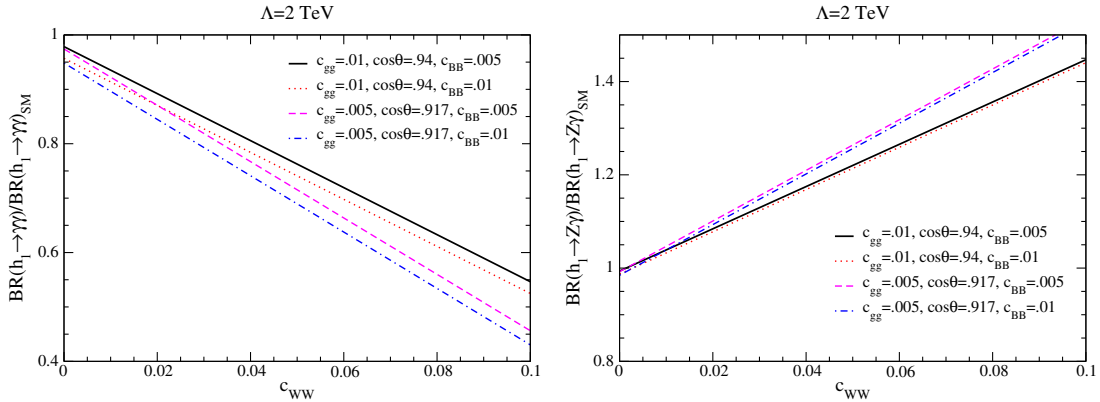
$$\begin{aligned}
 I_1(M_W) &= \int_0^{(m_1-M_W)^2} dq^2 \frac{q^2}{m_1^2} \left( 1 + \frac{1}{3} \frac{\hat{\lambda}(m_1^2, M_W^2, q^2)}{4q^2 M_W^2} \right) \frac{\hat{\lambda}^{1/2}(m_1^2, M_W^2, q^2)}{(q^2 - M_W^2)^2 + \Gamma_W^2 M_W^2} \\
 I_2(M_W) &= \int_0^{(m_1-M_W)^2} dq^2 \frac{q^2}{m_1^2} \frac{M_1^2 - M_W^2 - q^2}{2m_1^2} \frac{\hat{\lambda}^{1/2}(m_1^2, M_W^2, q^2)}{(q^2 - M_W^2)^2 + \Gamma_W^2 M_W^2} \\
 I_3(M_W) &= \int_0^{(m_1-M_W)^2} dq^2 \frac{q^2}{m_1^2} \frac{3(m_1^2 - M_W^2 - q^2)^2 - \hat{\lambda}(m_1^2, M_W^2, q^2)}{12m_1^4} \frac{\hat{\lambda}^{1/2}(m_1^2, M_W^2, q^2)}{(q^2 - M_W^2)^2 + \Gamma_W^2 M_W^2} \\
 \hat{\lambda}(x, y, z) &= (x - y - z)^2 - 4yz,
 \end{aligned} \tag{16}$$

$\tau_{1i} = \frac{4M_i^2}{m_1^2}$ , the coefficient  $\kappa$  is,

$$\begin{aligned}
 \kappa &= 3 \left( \left( \frac{1}{2} - s_W^2 \right)^2 + s_W^4 \right) + 3N_c \left( \left( -\frac{1}{2} + \frac{1}{3}s_W^2 \right)^2 + \frac{1}{9}s_W^4 \right) \\
 &\quad + 2N_c \left( \left( \frac{1}{2} - \frac{2}{3}s_W^2 \right)^2 + \frac{4}{9}s_W^4 \right) \\
 &= 3.68,
 \end{aligned} \tag{17}$$

with  $N_c = 3$  and  $s_W^2 = \sin^2 \theta_W = 1 - \frac{M_Z^2}{M_W^2}$ .

Some typical branching ratios of  $h_1$  into  $WW$  and  $ZZ$  normalized to the SM are shown in Fig. 3, and demonstrate little sensitivity to either  $c_{BB}$  or  $c_{WW}$  with subpercent level deviations. The branching ratios to  $\gamma\gamma$  and  $Z\gamma$  are shown in Fig. 4 and are very sensitive to  $c_{WW}$  and  $c_{BB}$ , changing upwards of 50% from the SM values. This is due to the SM rate first occurring at one loop. We note that in the limit  $c_{gg} = c_{WW} = c_{BB} = 0$ , all of the branching ratios are equal to their SM values for  $\sin \theta = 0$ , and the deviations from 1 in Figs. 3 and 4 are a result of the interplay between the singlet mixing and the EFT operators. These figures retain only the linear terms in the EFT couplings, as we have

FIG. 4. Branching ratios for (left-hand side)  $h_1 \rightarrow \gamma\gamma$ , and (right-hand side)  $h_1 \rightarrow Z\gamma$  for representative values of the parameters.

implicitly assumed  $s_\theta$  is small and we note that the  $c_i^2$  coefficients are always suppressed by  $s_\theta^2$  for  $h_1$  production [see Eq. (15)].

For completeness, we note that the hadronic cross section for production of  $h_1$  or  $h_2$  from gluon fusion is

$$\sigma(pp \rightarrow h_i) = \frac{\pi^2}{8m_i S_H} \Gamma(h_i \rightarrow gg) L \quad (18)$$

where

$$L = \int_{\ln(\sqrt{\zeta})}^{-\ln(\sqrt{\zeta})} dy g(\sqrt{\zeta} e^y) g(\sqrt{\zeta} e^{-y}), \quad (19)$$

$\sqrt{S_H}$  is the hadronic center-of-mass energy and  $\zeta = m_i^2/S_H$ .

### III. CONSTRAINTS FROM $h_1$

The measurements of SM Higgs couplings place stringent restrictions on the allowed parameters of the model. Both ATLAS and CMS limit the mixing angle,  $\theta$ , in the singlet model in the case  $c_{gg} = c_{WW} = c_{BB} = 0$ , as discussed in the previous section. These limits are significantly affected by the addition of the EFT operators. We fit to the parameters of our model using the combined ATLAS/CMS 8 TeV results [15]. The simplest possible limit is obtained by a fit to the overall gluon fusion signal strength for  $h_1$ ,

$$\mu_{ggF} = 1.03^{+0.17}_{-0.15}. \quad (20)$$

The 95% confidence level limit from the  $ggF$  signal strength is shown in Fig. 5. This fit demonstrates the cancellations between the contributions of the singlet model and the contributions of the EFT coefficients. For  $s_\theta = 0$ , the EFT operators do not contribute to  $h_1$  decay, and so there is no limit on  $c_{gg}$  (the lower band extending across all  $c_{gg}$  values). For  $s_\theta = 1$ , the SM contributions vanish, and the observed  $h_1$  production rate is obtained by adjusting  $c_{gg}$  (we have only plotted allowed values). For small  $c_{gg}$ , we observe the interplay of the mixing and EFT contributions, and larger values of  $s_\theta$  are allowed than in the  $c_{gg} = 0$  limit. In this plot, we retain only the linear contributions in  $c_{gg}$ . If the  $c_{gg}^2$  terms become numerically relevant, then the dimension-6 terms must be included in the EFT of Eq. (5).

In Fig. 5, we also fit the  $h_1$  coupling strengths [15] using the 6 parameter fit to the  $gg$  initial state at 8 TeV,

$$\begin{aligned} \mu_F^{\gamma\gamma} &= 1.13^{+0.24}_{-0.21} & \mu_F^{WW} &= 1.08^{+0.22}_{-0.19} \\ \mu_F^{ZZ} &= 1.29^{+0.29}_{-0.25} & \mu_F^{bb} &= .66^{+0.37}_{-0.28} \\ \mu_F^{\tau\tau} &= 1.07^{+0.35}_{-0.28}. \end{aligned} \quad (21)$$

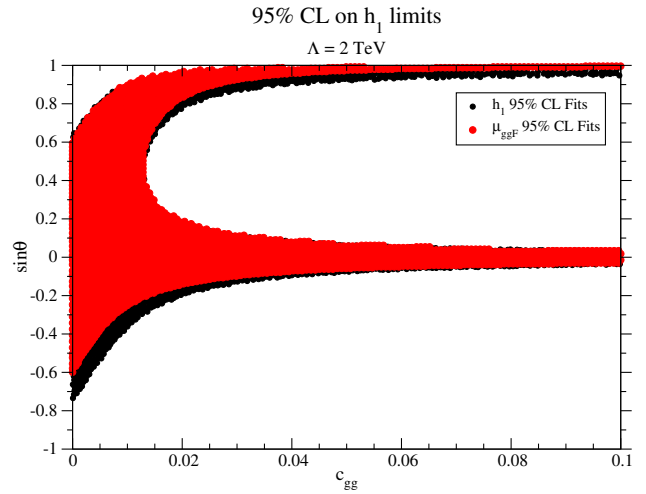


FIG. 5. 95% confidence level allowed regions using the gluon fusion signal strength for  $h_1$  production (red) and allowed regions derived from fits to the signal strengths given in Eq. (21) (black) [15] with  $\Lambda = 2$  TeV. Only the linear terms in the EFT expansion are included.

These are labeled as “ $h_1$  95% C.L. fits.” The results of the two fits are quite similar.

### IV. CONSTRAINTS FROM $h_2$

We turn now to a joint examination of the measured properties of the  $h_1$  as given in Eq. (21) and the experimental limits on heavy resonances shown in Tables I and II for heavy scalars with masses of  $m_2 = 400, 600$  and  $750$  GeV decaying to SM particles using the results of Eq. (11). We calculate the signal rates at leading order in QCD and normalize to the recommended values for the SM production rates from the LHC Higgs Cross Section Working Group [22] given in Table III.

Figure 6 shows the regions excluded from the restrictions from resonance searches at 8 TeV and 13 TeV. For  $\sin \theta = 0$ , there is now an upper limit to  $c_{gg}$  that arises from the dijet searches. The region at  $\sin \theta = 1$ , present in the  $h_1$  fits, largely vanishes at  $m_2 = 600$  and  $750$  GeV, and is greatly reduced at  $m_2 = 400$  GeV. The excluded region

TABLE I. 95% C.L. LHC limits on  $\sigma \cdot BR$  for heavy resonances at  $\sqrt{S_H} = 8$  TeV. Asterisks indicate that there are no current bounds in these channels.

Channel	$m_2 = 400$ GeV	$m_2 = 600$ GeV	$m_2 = 750$ GeV
$WW$	0.362 pb [23]	0.118 pb [23]	0.0361 pb [23]
$ZZ$	0.0648 pb [24]	0.0218 pb [24]	0.0118 pb [24]
$t\bar{t}$	*	1.2 pb [25]	0.71 pb [25]
$Z\gamma$	0.00720 pb [26]	0.00296 pb [26]	0.00402 pb [26]
$\tau^+\tau^-$	0.087 pb [27]	0.020 pb [27]	0.012 pb [27]
$j\bar{j}$	*	3.76 pb [28]	1.79 pb [28]
$h_1 h_1$	0.442 pb [29]	0.137 pb [29]	0.0498 pb [29]
$\gamma\gamma$	0.00215 pb [30]	0.000666 pb [31]	0.00129 pb [30]



TABLE II. 95% C.L. LHC limits on  $\sigma \cdot BR$  for heavy resonances at  $\sqrt{s_H} = 13$  TeV. Asterisks indicate that there are no current bounds in these channels.

Channel	$m_2 = 400$ GeV	$m_2 = 600$ GeV	$m_2 = 750$ GeV
WW	1.4 pb [32]	0.5 pb [32]	0.31 pb [32]
ZZ	0.210 pb [33]	0.083 pb [34]	0.043 pb [34]
$Z\gamma$	0.041 pb [35]	.013 pb [35]	0.010 pb [35]
$\tau^+\tau^-$	0.27 pb [36]	0.053 pb [36]	0.030 pb [36]
$jj$	*	21.4 pb [37]	9.54 pb [37]
$h_1 h_1$	5.9 pb [38]	1.6 pb [38]	0.85 pb [38]
$\gamma\gamma$	0.0018 pb [39]	0.0015 pb [39]	0.00068 pb [39]
$b\bar{b}$	*	5.1 pb [40]	5.2 pb [40]

TABLE III. Theoretical cross sections at NNLO + NNLL for heavy scalar resonances from the LHC Higgs Cross Section Working Group [22].

	8 TeV, $\sigma(pp \rightarrow h_2)$	13 TeV, $\sigma(pp \rightarrow h_2)$
$m_2 = 400$ GeV	3.01 pb	9.52 pb
$m_2 = 600$ GeV	0.52 pb	2.01 pb
$m_2 = 750$ GeV	0.15 pb	0.64 pb

shows little sensitivity to the parameter of the scalar potential. The counting of small parameters is different for the  $h_2$  decays than in the  $h_1$  case. If we treat both  $s_\theta$  and  $c_i$  as small parameters, then the  $c_i^2$  contributions to  $h_2$  decays are of the same order as the terms independent of the  $c_i$ . Hence for the  $h_2$  decays, we include the  $c_i^2$  contributions.

In Fig. 7, we plot the regions allowed by both  $h_1$  coupling fits and resonance searches. We see that the large  $c_{gg}$  regions that are allowed by the coupling constant fits are eliminated by the resonance search limits for  $m_2 = 600$  GeV and 750 GeV. Considering all constraints, for  $m_2 = 600$  and 750 GeV we find  $|\sin \theta| \lesssim 0.6$ . For  $m_2 = 400$  GeV, the resonance searches are less restrictive for positive  $\sin \theta$  and the limit is  $\sin \theta \gtrsim -0.4$ . For all masses these limits are much weaker than  $|\sin \theta| \leq 0.35$  [14] in the renormalizable model without the EFT operators in Eq. (5).

Finally, requiring a narrow width  $\Gamma(h_2)/m_2 < 5\%$ , where  $\Gamma(h_2)$  is the total  $h_2$  width, further constrains the allowed regions of  $\sin \theta$ . For  $m_2 = 600$  and 750 GeV the limit is  $|\sin \theta| \lesssim 0.4$ . For  $m_2 = 400$  GeV, the effect of the narrow width restriction is to eliminate the large  $\sin \theta \sim 1$  region. The remaining parameter region is  $-0.4 \lesssim \sin \theta \lesssim 0.7$ .

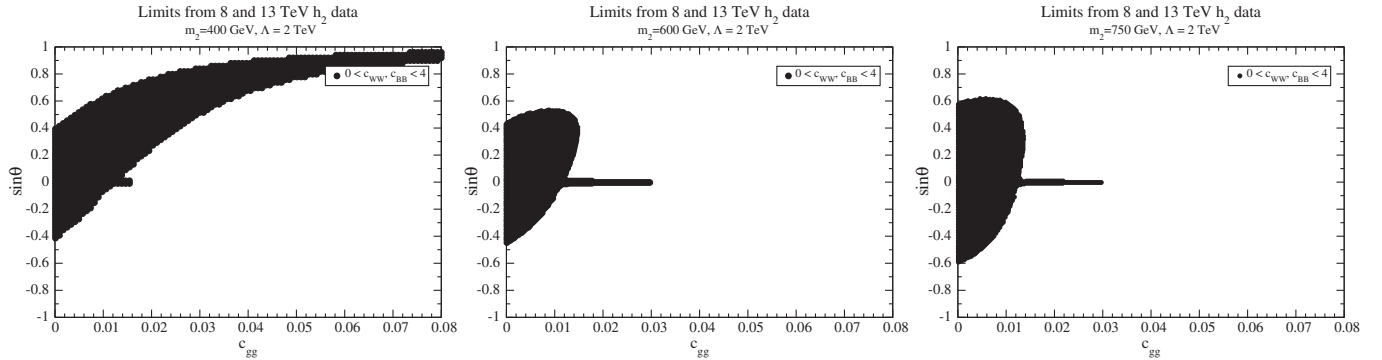


FIG. 6. 95% confidence level allowed regions obtained by varying  $c_{gg}$ ,  $c_{WW}$ ,  $c_{BB}$ ,  $\cos \theta$ , along with  $b_1$ ,  $b_3$  and  $a_2$ , allowed by the 8 TeV and 13 TeV resonance searches of Tables I and II.

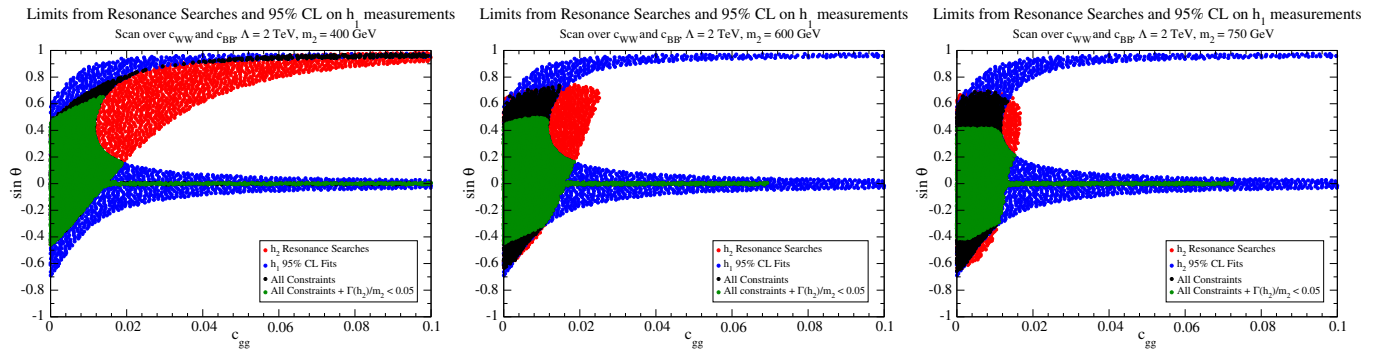


FIG. 7. Allowed regions combining  $h_1$  and  $h_2$  data and a narrow width  $\Gamma(h_2)/m_2 < 0.05$  restriction. The new physics scale is set  $\Lambda = 2$  TeV, and  $c_{WW}$ ,  $c_{BB}$  are scanned over.

## V. CONCLUSIONS

We examined the effects on Higgs physics of a gauge singlet scalar which mixes with the SM-like 125 GeV Higgs boson when the theory is augmented by EFT operators coupling the singlet scalar to SM gauge bosons. The new feature of our analysis is a study of the properties of both the 125 GeV and heavy scalar resonance, and the demonstration that significant cancellations are possible between effects in the two sectors. We fit our model parameters to the 7 and 8 TeV combined ATLAS and CMS precision Higgs measurements [15] and applied constraints from scalar resonance searches at the 8 and 13 TeV LHC.

We find that the inclusion of the operators greatly changes the allowed values of the scalar mixing angle. In the renormalizable model, the strongest bound from Higgs precision is  $|\sin \theta| \leq 0.35$  [14]. Including the EFT

operators between the singlet scalar and SM gauge bosons, we find Higgs precision measurements and scalar resonance searches give  $\sin \theta \gtrsim -0.4$  for a heavy scalar mass of 400 GeV and  $|\sin \theta| \lesssim 0.6$  for masses of 600 and 750 GeV. If the additional requirement of a narrow width  $\Gamma(h_2)/m_2 < 0.05$  is included, the limits are  $-0.4 \lesssim \sin \theta \lesssim 0.7$  for a heavy scalar mass of 400 GeV and  $|\sin \theta| \lesssim 0.4$  for masses of 600 and 750 GeV. In all cases, these restrictions are less than those in the renormalizable theory.

Digital data related to our results can be found at [41].

## ACKNOWLEDGMENTS

This work is supported by the U.S. Department of Energy under Grant No. DE-SC0012704. We thank Chien-Yi Chen for many valuable discussions about the singlet model.

- 
- [1] J. R. Espinosa, T. Konstandin, and F. Riva, Strong electroweak phase transitions in the standard model with a singlet, *Nucl. Phys.* **B854**, 592 (2012).
  - [2] S. Profumo, M. J. Ramsey-Musolf, and G. Shaughnessy, Singlet Higgs phenomenology and the electroweak phase transition, *J. High Energy Phys.* **08** (2007) 010.
  - [3] S. Profumo, M. J. Ramsey-Musolf, C. L. Wainwright, and P. Winslow, Singlet-catalyzed electroweak phase transitions and precision Higgs boson studies, *Phys. Rev. D* **91**, 035018 (2015).
  - [4] D. Curtin, P. Meade, and C.-T. Yu, Testing electroweak baryogenesis with future colliders, *J. High Energy Phys.* **11** (2014) 127.
  - [5] M. Perelstein and Y.-D. Tsai, 750 GeV Di-photon excess and strongly first-order electroweak phase transition, *Phys. Rev. D* **94**, 015033 (2016).
  - [6] D. O'Connell, M. J. Ramsey-Musolf, and M. B. Wise, Minimal extension of the standard model scalar sector, *Phys. Rev. D* **75**, 037701 (2007).
  - [7] V. Barger, P. Langacker, M. McCaskey, M. Ramsey-Musolf, and G. Shaughnessy, Complex singlet extension of the standard model, *Phys. Rev. D* **79**, 015018 (2009).
  - [8] G. Marco Pruna and T. Robens, The Higgs singlet extension parameter space in the light of the LHC discovery, *Phys. Rev. D* **88**, 115012 (2013).
  - [9] C.-Y. Chen, S. Dawson, and I. M. Lewis, Exploring resonant di-Higgs boson production in the Higgs singlet model, *Phys. Rev. D* **91**, 035015 (2015).
  - [10] T. Robens and T. Stefaniak, LHC benchmark scenarios for the real Higgs singlet extension of the standard model, *Eur. Phys. J. C* **76**, 268 (2016).
  - [11] S. Dawson and I. M. Lewis, NLO corrections to double Higgs boson production in the Higgs singlet model, *Phys. Rev. D* **92**, 094023 (2015).
  - [12] R. Costa, M. Mhlleitner, M. O. P. Sampaio, and R. Santos, Singlet extensions of the standard model at LHC run 2: benchmarks and comparison with the NMSSM, *J. High Energy Phys.* **06** (2016) 034.
  - [13] A. Ahriche, What is the criterion for a strong first order electroweak phase transition in singlet models?, *Phys. Rev. D* **75**, 083522 (2007).
  - [14] G. Aad *et al.*, Constraints on new phenomena via Higgs boson couplings and invisible decays with the ATLAS detector, *J. High Energy Phys.* **11** (2015) 206.
  - [15] ATLAS Collaboration, Technical Report No. ATLAS-CONF-2015-044, CERN, Geneva, 2015.
  - [16] S. Dawson and W. Yan, Hiding the Higgs boson with multiple scalars, *Phys. Rev. D* **79**, 095002 (2009).
  - [17] M. Bauer, A. Butter, J. Gonzalez-Fraile, T. Plehn, and M. Rauch, Learning from the new Higgs-like scalar before it vanishes, [arXiv:1607.04562](#).
  - [18] K. Cheung, P. Ko, J. Sik Lee, J. Park, and P.-Y. Tseng, Double Higgscision: 125 GeV Higgs boson and a potential diphoton resonance, [arXiv:1608.00382](#).
  - [19] J. F. Gunion, H. E. Haber, G. L. Kane, and S. Dawson, The Higgs hunter's guide (Brookhaven National Laboratory, Upton, NY, 1989).
  - [20] A. Djouadi, The anatomy of electro-weak symmetry breaking. I: The Higgs boson in the standard model, *Phys. Rep.* **457**, 1 (2008).
  - [21] R. Contino, M. Ghezzi, C. Grojean, M. Mhlleitner, and M. Spira, eHDECAY: An implementation of the Higgs effective lagrangian into HDECAY, *Comput. Phys. Commun.* **185**, 3412 (2014).
  - [22] LHC Higgs Cross Section Working Group, Handbook of LHC Higgs cross sections: 3. Higgs properties, edited by S. Heinemeyer, C. Mariotti, G. Passarino, and R. Tanaka, [arXiv:1307.1347](#).
  - [23] G. Aad *et al.*, Search for a high-mass Higgs boson decaying to a  $W$  boson pair in  $pp$  collisions at  $\sqrt{s} = 8$  TeV with the ATLAS detector, *J. High Energy Phys.* **01** (2016) 032.



- [24] G. Aad *et al.*, Search for an additional, heavy Higgs boson in the  $H \rightarrow ZZ$  decay channel at  $\sqrt{s} = 8$  TeV in  $pp$  collision data with the ATLAS detector, *Eur. Phys. J. C* **76**, 45 (2016).
- [25] G. Aad *et al.*, A search for  $t\bar{t}$  resonances using lepton-plus-jets events in proton-proton collisions at  $\sqrt{s} = 8$  TeV with the ATLAS detector, *J. High Energy Phys.* **08** (2015) 148.
- [26] G. Aad *et al.*, Search for new resonances in  $W\gamma$  and  $Z\gamma$  final states in  $pp$  collisions at  $\sqrt{s} = 8$  TeV with the ATLAS detector, *Phys. Lett. B* **738**, 428 (2014).
- [27] G. Aad *et al.*, Search for neutral Higgs bosons of the minimal supersymmetric standard model in  $pp$  collisions at  $\sqrt{s} = 8$  TeV with the ATLAS detector, *J. High Energy Phys.* **11** (2014) 056.
- [28] V. Khachatryan *et al.*, Search for Narrow Resonances in Dijet Final States at  $\sqrt{s} = 8$  TeV with the MoveL CMS Technique of Data Scouting, *Phys. Rev. Lett.* **117**, 031802 (2016).
- [29] V. Khachatryan *et al.*, Search for resonant pair production of Higgs bosons decaying to two bottom quark–antiquark pairs in proton–proton collisions at 8 TeV, *Phys. Lett. B* **749**, 560 (2015).
- [30] V. Khachatryan *et al.*, Search for diphoton resonances in the mass range from 150 to 850 GeV in  $pp$  collisions at  $\sqrt{s} = 8$  TeV, *Phys. Lett. B* **750**, 494 (2015).
- [31] G. Aad *et al.*, Search for Scalar Diphoton Resonances in the Mass Range 65–600 GeV with the ATLAS Detector in  $pp$  Collision Data at  $\sqrt{s} = 8$  TeV, *Phys. Rev. Lett.* **113**, 171801 (2014).
- [32] ATLAS Collaboration, CERN, Technical Report No. ATLAS-CONF 074, 2016.
- [33] CMS Collaboration, CERN, Technical Report No. CMS-PAS-HIG 033, 2016.
- [34] ATLAS Collaboration, CERN, Technical Report No. ATLAS-CONF 056, 2016.
- [35] ATLAS Collaboration, CERN, Technical Report No. ATLAS-CONF 044, 2016.
- [36] ATLAS Collaboration, CERN, Technical Report No. ATLAS-CONF 085, 2016.
- [37] CMS Collaboration, CERN, Technical Report No. CMS-PAS-EXO 032, 2016.
- [38] CMS Collaboration, CERN, Technical Report No. CMS-PAS-HIG 029, 2016.
- [39] ATLAS Collaboration, CERN, Technical Report No. ATLAS-CONF 059, 2016.
- [40] CMS Collaboration, CERN, Technical Report No. CMS-PAS-HIG 025, 2016.
- [41] [https://quark.phy.bnl.gov/Digital\\_Data\\_Archive/dawson/singlet\\_16/](https://quark.phy.bnl.gov/Digital_Data_Archive/dawson/singlet_16/).